Microstructured Radiators

Final Report

Authors: Jean-Jacques Greffet, Marine Laroche, François Marquier
Affiliation: Ecole Centrale Paris

ESA Researcher(s): Luzi Bergamin

Date: 01.07.2007

Contacts:

Jean-Jaques Greffet
Tel: +33 (0) 1 41 13 10 61
Fax: +33 (0) 1 47 02 80 35
e-mail: pba@univ-nantes.fr

Leopold Summerer
Tel: +31(0)715655174
Fax: +31(0)715658018
e-mail: act@esa.int

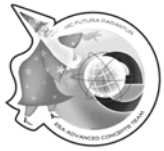

Available on the ACT website
http://www.esa.int/act

Ariadna ID: 06/9501b
Study Duration: 2 months
Contract Number: 20303/06/NL/HE

Contents

1 Introduction

Radiative cooling and directional heating are key issues for the control of thermal management in spatial applications. Depending on its role on the satellites, two types of radiators will have to be designed. For radiative cooling, the best performances will be achieved with an isotropic emission pattern for a wavelength range corresponding to the maximum of Planck's function at a given temperature. For directional heating, a spatially coherent thermal source will be optimized.

Throughout the study, we will equivalently refer to absorptivity and to emissivity since the equality of the absorptivity and emissivity will be demonstrated by a rigorous derivation of Kirchhoff's law, using the reciprocity theorem of electromagnetism (see Appendix A). This confirms the validity of using numerical simulations which derive the absoprtion by a system illuminated by a plane wave. This yields the polarized directional monochromatic absorptivity which is equal to the polarized directional monochromatic emissivity.

A direct calculation of the emission in the framework of electromagnetism can as well be done. This Langevin type approach, originally introduced in the context of radiowaves [1] has been used to compute the emission of light in the visible or the infrared. Several properties of the emitted field in the near-field have been discovered [2, 3]. Of particular interest in the context of emission is that the coherence length was shown to be much smaller than the wavelength for all the materials that do not support a surface wave [2, 4]. Thus, different surface elements radiate fields that do not interfere even if they are separated by distances smaller than the wavelength. This is far from trivial since the coherence length of the blackbody radiation is $\lambda/2$ [5]. In other words, emitted radiation close to a surface is less coherent than blackbody radiation. It is thus justified to consider that different volume elements of a given opaque material are incoherent radiation sources. We will show that this property provides a foundation for the application of the usual phenomenological modelling of thermal emission on a length scale smaller than the wavelength. The above properties are valid only if surface waves such as surface phonon polaritons or surface plasmon polaritons cannot propagate along the interface. When surface waves can be excited, they dominate all the surface properties as shown recently for Casimir forces [6] and for the energy density close to an interface [7]. In the context of emission of light,

the coherence length of the emitted field plays a crucial role. It has been shown that the coherence length is essentially the decay length of the surface wave and can therefore be much larger than the wavelength [2]. In the presence of a grating, this can modify dramatically the emission of light as demonstrated in Ref. [8–10].

Section 2 will be devoted to the study of the different physical mechanisms leading to an enhancement of the emission of microstructured radiators. Then, the interesting case of microstructured radiators in the resonant regime will be analysed in section 3. Section 5 will consider the scalability and robustness of the radiators if integrated on a satellite. Finally, section 4 will give some examples of calculations of the emission pattern of microstructures made of aluminium.

In order to compute the radiative properties of the microstructured materials throughout the study, we will use as a reference numerical simulations of scattering of electromagnetic waves by gratings [11]. Recent progress has considerably improved the convergence of algorithms based on modal techniques for gratings [12, 13]. We use an algorithm proposed by Chateau and Hugonin [14]. This technique, called Rigourous Coupled Wave Algorithm (RCWA), is numerically stable so that it allows to deal with gratings with arbitrary period and depth.

2 Absorption by surfaces: Overview of the physical mechanisms.

The emissivity of a surface (defined in appendix A) is not an intrinsic property of the material. Yet, a slight modification of the surface of a radiator can dramatically change its emission pattern. The motivation of this section is to highlight all the physical mechanisms responsible for an increase of emissivity of microstructured radiators. Depending on the scale of the microstructures, we will identify three different regimes of absorption depending on the ratio of the wavelength and the period of the roughness (or microstructures):

1. the homogenization regime : it occurs when the pertubation has a transverse length-scale much smaller than the wavelength.

2. the geometrical optics regime : it corresponds to the case of perturbations much larger than the wavelength so that the classical ray optics description is valid.

3. the resonant regime : this describes the case of microstructures with the same length-scale as the wavelength.The particular case of microstructured radiators will be adressed in section 3, as well as the phenomenon of coherent thermal emission.

We will show that absorptivity can become very large in each regime owing to different mechanisms. All of them can be used to design efficient radiators

2.1 A review of the different regimes.

2.1.1 Homogenization regime.

When the wavelength is much larger than the period of the microstructure, it is possible to consider that the wave sees an effective homogeneous medium characterized by an effective index [15–17]. For a s-polarized field illuminating a 2D grating, the effective dielectric constant is given by the average of the dielectric constant of the components weighted by their volume filling fraction f. For an

interface between a medium of dielectric constant ϵ_1, and filling factor f and air, we have

$$\epsilon_{eff} = f\epsilon_1 + (1-f)\epsilon_{air} \tag{1}$$

For *p*-polarization, at normal incidence, one has to average the inverse of ϵ.

$$(\epsilon_{eff})^{-1} = f(\epsilon_1)^{-1} + (1-f)(\epsilon_{air})^{-1} \tag{2}$$

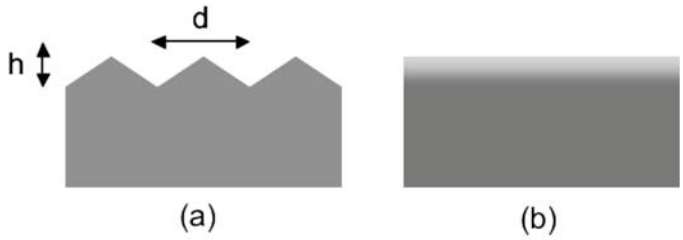

Figure 1: Schematic view of a periodic surface profile and its equivalent in the homogenization regime. (a) sawtooth profile, (b) gradient profile equivalent to a sawtooth profile. The period is denoted by d, the height by h.

In the case of a sawtooth profile, the effective index depends on z because the filling factor depends on z (see figure 1). Therefore, there is a gradient of effective index. This gradient is the origin of the mechanism of the antireflective behaviour of the grating. The origin of this antireflection is simply the destructive interferences between the waves reflected by the multilayer system (equivalent to the index gradient). To check this explanation, we have computed the absorptivity of a system with an index gradient. This can be done by replacing the continuous system by a multilayer system. A standard matrix approach can then be used to find the reflectivity and absorptivity of the system. We have found that the RCWA tends to this value whereas the ray tracing result was clearly wrong (not shown). We have summarized the results of a comparison between the homogenization model and the RCWA results in table 1 for two materials and two polarizations. We have found that there is always a good agreement when the period is smaller than 0.4λ.

We now address the question of the enhancement of the emissivity when dealing with the homogenization regime. The answer can be borrowed from the classical work on index gradient. It is known that there are different profiles that can

h/λ	material	RCWA *s*	Homogenization *s*	RCWA *p*	Homogenization *p*
0.1	Au	0.24	0.24	0.85	0.83
0.1	W	0.62	0.62	0.69	0.71
1	Au	0.52	0.52	0.99	0.99
1	W	0.9	0.9	0.99	0.99

Table 1: Emissivity computed using the RCWA method and the matrix method for multilayered system with an effective index. The angle of emission is 1^o and the ratio d/λ is 0.05. The grating has a symetric sawtooth profile.

achieve a zero reflection. Analytical solutions are available for some particular profiles [18]. When working in the homogenization regime, a minimum depth is necessary to ensure that reflectivity decreases. It is usually on the order of the wavelength. Let us mention that it has been shown that the quintic profile (fifth-order dependence on depth of a graded refractive-index profile) has been shown to be very efficient for this purpose [19, 20].

2.1.2 Geometrical optics regime

The regime of geometrical optics occurs when the period of the microstructure is very large compared to the wavelength so that the ray tracing approach holds.

Derivation of the emissivity using geometrical optics

A calculation based on geometrical optics assumes that the concept of ray can be used. A direct derivation of the emissivity can be done as follows. We first choose an emitted ray characterized by both its direction and its position x in the surface plane. A backwards ray tracing can be done using the reflection laws. At each intersection with the surface, we can take into account the emission and reflection process using the Fresnel reflection factors. It is thus an easy matter to recover the contribution to the emission of this particular ray. Averaging over all possible rays over the surface yields the final emissivity. Let us consider as an example a ray that undergoes two reflections. The energy emitted can be written as

$$\begin{aligned}\epsilon(x) &= \epsilon_3 R_1 R_2 + \epsilon_2 R_1 + \epsilon_1 &(3)\\ &= (1-R_3)R_1R_2 + (1-R_2)R_1 + 1 - R_1 &(4)\\ &= 1 - R_1R_2R_3. &(5)\end{aligned}$$

It is simple to generalize this form to a ray undergoing N reflections, its emissivity being $1 - R_1R_2 \ldots R_N$.

An alternative calculation can be done based on the absorptivity. It yields the same result. We first choose a particular incident ray characterized again by its direction and its intersection with the horizontal plane. A ray tracing procedure is then used. At each reflection event, a fraction $1 - R_n$ of the energy of the beam is absorbed so that the remaining energy is simply proportional to R_n. After N reflection events, the remaining energy is proportional to $R_1R_2 \ldots R_N$. The absorptivity is thus $1 - R_1R_2 \ldots R_N$. We find the same expression than for the emissivity.

So far, we have evaluated the contribution of a ray that impinges on the surface at a particular point x. The next step is to average the emissivity over the surface. If we consider a grating of period d, the average reads :

$$\epsilon = \frac{1}{d}\int_0^d \epsilon(x)\mathrm{d}x \tag{6}$$

We have now to discuss the validity of this approach. A priori, this concept can be used as far as there is no diffraction phenomena. But we will see in the next section that its range of validity can be larger in some cases.

Mechanism of enhancement of the emissivity

We start by considering the emissivity of a grating with a sawtooth profile (see Fig. 1) illuminated under an angle of incidence of 1^o. In order to study the different regimes, we vary the period of the grating (d) in the range $[\lambda/20, 25.6\lambda]$. Figure 2a shows the emissivity for a height equal to 0.1λ of a tungsten grating in *s*-polarization. We do not expect multiple scattering and shadowing for this grating except possibly for very small periods. It is seen that the ray tracing approach yields the same result as the RCWA for large periods but fails for periods smaller

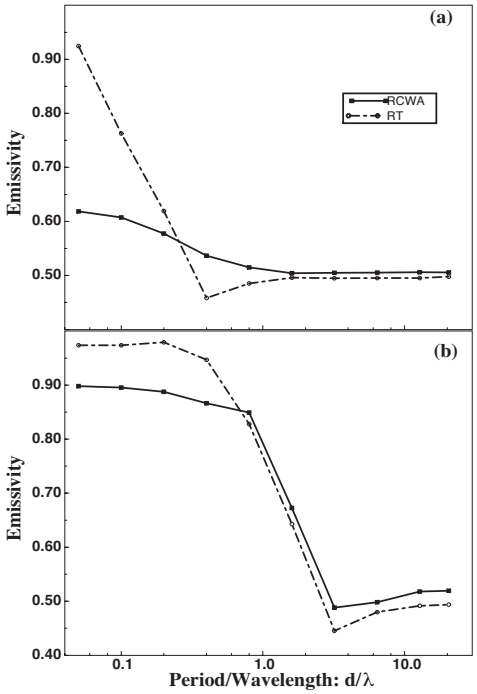

Figure 2: Dependence of the *s*-polarized emissivity on the period of the surface profile. Optical index of tungsten at 0.55 μm, $n = 3.5 + i2.73$, $\theta = 1^o$, (a) $h = 0.1\lambda$, (b) $h = \lambda$

than $d/\lambda = 0.8$. A similar result is observed for a height of the grating equal to one wavelength (see Fig. 2b). Thus we find that the wave approach and the ray tracing approach agree very well for relatively small periods, whereas already in the resonance regime.

We now turn to the case of *p*-polarization. It is seen in Fig. 3 that there is no agreement in the resonance region. It is necessary to have periods larger than 2λ to observe a good agreement. This is not surprising. It is kown that the lateral extension of the fields scattered by a surface defect is larger in *p*-polarization than in *s*-polarization. This was called short range coupling by D. Maystre [21] who noticed that the coupling range in *p*-polarization was larger than in *s*-polarization. It seems that the value of the period that we find is similar to the coupling ranges

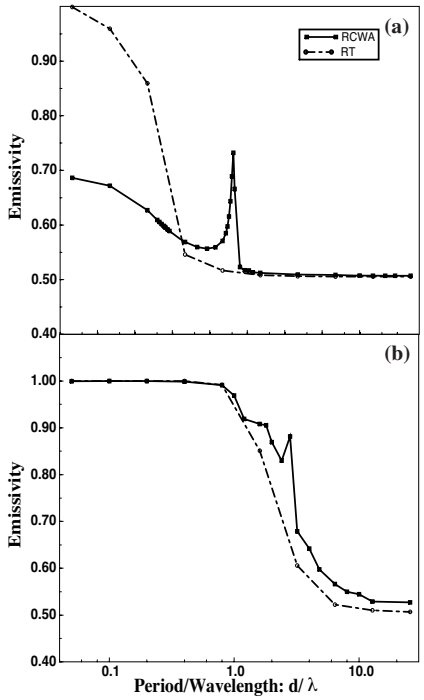

Figure 3: Dependence of the *p*-polarized emissivity on the period of the surface profile. Same parameters. (a) $h = 0.1\lambda$, (b) $h = \lambda$.

defined by Maystre.

We now turn to a grating illuminated with an angle of incidence of 60^o for *p*-polarization. Again, we consider two heights, $h = 0.1\lambda$ and $h = \lambda$. Results are displayed in Figure 4. For small height (Fig. 4a) and therefore small slopes, the ray tracing approach yields good results up to $d/\lambda = 1$ whereas for the case $h = \lambda$ (Fig. 4b), there is no agreement for any period. In the latter case, there is shadowing at any angle preventing the technique to yield reliable results.

We now discuss the mechanism of enhancement of the emissivity. In Fig. 2a, we find that the emissivity is essentially the emissivity of a bare flat surface. It is seen on Fig. 2b that the emissivity increases substantially as the period decreases. The mechanism responsible for this enhancement of the emissivity is very simple. Since there is multiple scattering, (or ray trapping) there is more absorption. We

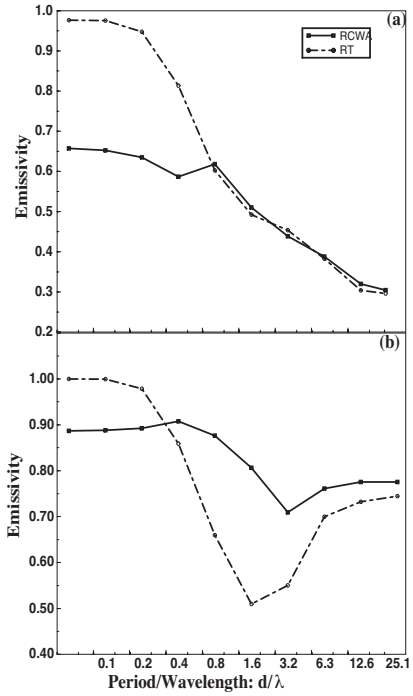

Figure 4: Influence of the angle of incidence on the validity of ray tracing. $0.55\ \mu$m, $n = 3.5 + i2.73$, $\theta = 60^o$, (a) $h = 0.1\lambda$, (b) $h = \lambda$

may call this a cavity effect.

2.1.3 Resonance regime

The resonance regime can be considered to be the regime where both the homogenization and the ray tracing approaches fail. It corresponds roughly to values of the period between $\lambda/4$ and $\lambda - 5\lambda$ depending on the polarization and the surface profile. We have already emphasized that for angles of incidence larger than the maximum slope of the sample, so-called shadowing effects appear so that ray tracing ceases to be accurate. Thus an accurate definition of the resonance domain should take into account the angle of incidence.

Besides these limitations, *the resonance regime is the regime where surface*

waves or any other kind of resonances of the structure modify the emissivity.

Part 3 will be devoted to the study of the resonance regime. In particular, we will emphasize the different kinds of resonance that can be excited in microstrutured radiators. We will also explain why the excitation of such resonances lead to an enhancement of the thermal emission as well as an different angular emission pattern.

In conclusion, we have described three different regimes depending on the ratio d/λ. For values of d/λ smaller than $1/2$,the emissivity of the rough surface is well described by an effective homogeneous index. This is the homogenization regime. For values of d/λ larger than 2, the ray tracing model is valid provided that there is no shadowing and no excitation of surface waves. In the intermediate regime or resonance regime that corresponds to a period on the order of the wavelength, it is well-known that the scattering cannot be described by geometrical optics. Although one expects the ray tracing approach to break down due to wave effects, it turns out that the emissivity of the surface is very well acounted for in many cases. When no shadowing and no surface waves effects exist, the region where ray tracing fails corresponds to periods smaller than 2 wavelengths. For the two extreme regime ($d > \lambda$ and $d << \lambda$), we have shown that the emissivity can be enhanced. Within the ray tracing approach, a large absorptivity can be obtained by a cavity or ray trapping effect. In the homogenization regime, a large absorptivity follows from the index gradient that reduces reflection.

Let us now consider the resonance regime, and in particular the case in which we are interested in : the enhancement of the emission of microstructured radiators and the conditions for isotropic or directional emission.

3 Review of microstructured radiators

In this section, we focus on the modification of radiative properties of microstructured radiators comparing to plane interfaces. Actually we study thermal sources in the resonance regime. We first discuss the concept of coherent thermal emission. Then, we give a review of existing solutions to yield coherent thermal radiators as well as other kind of microstructured radiators.

3.1 Introduction to coherent thermal emission

In this section, we explain the physical origin of coherent thermal emission via surface waves. Let us first say a few words on the mechanism of thermal emission. The tungsten filaments that are used in light bulbs are certainly the most widely used sources of light. We will call such sources thermal sources of light. The mechanism of light generation is spontaneous emission. They are an almost isotropic source of light with a broad spectrum. This contrasts with a laser that produces a very directional and monochromatic light. The narrow spectrum is a measure of the temporal coherence of the source whereas the directivity is a measure of its spatial transverse coherence (see Appendix C). Recently, it has been realized [2–4] that a thermal source of light could be coherent in the near field, i.e. when analysing the light at distances of the surface smaller than the peak wavelength of the spectrum. Further work has led to the construction of a coherent source of thermal light [9]. It has thus been shown that a source based on spontaneous emission may produce light partially spatially coherent.

The emission of light by hot bodies is usually discussed in the context of energy transfer or thermodynamics using phenomenological concepts such as absorptivity, emissivity and specific intensity [22, 23]. However, it is possible to address this problem in the framework of classical electrodynamics. This approach was first used by Lorentz but at that time, the statistical properties of the random currents were not known so that it was impossible to obtain the Planck function following this path [1]. This is why this type of approach had disappeared and had been replaced by two complementary approaches. Radiation in a vacuum,

[1] Thermal motion of electrons or atoms are at the origin of thermal radiation. This motion of charged particles or atoms with different electronegativity involves random currents in the material so that random currents can be seen as the origin of thermal emission

i.e. black body radiation, is derived using the Bose Einstein statistics for photons. Emission by a specific material is described using a phenomenological theory.

The basic idea of an electromagnetic treatment of thermal radiation is that each volume element of a body at temperature T can be viewed as an electromagnetic dipole. Indeed, because of the random thermal motions of electrons and ions, there are random induced currents in the material. Therefore, each volume element generates an electric field. Because the mean value of the current is null, the mean value of the electric field is also null. The quantity that is then needed is the correlation function of the current density which is given by the fluctuation-dissipation theorem derived in 1948. The full treatment has been first given by Rytov [24]. It has been applied by these authors mostly to radio waves emission problems but the framework is valid for any frequency. This approach allows to derive rigorously the emissivity for a flat surface and thus to retrieve the usual phenomenological result widely used. Yet, it allows also to derive the field in the vicinity of the interface. It has been shown that when surface waves can exist (see Appendix B for an introduction to surface waves), the field is completely dominated by these surface waves thermally excited producing unexpected results. First of all, the spectrum of the energy density becomes almost monochromatic. Secondly, the density of energy increases by several orders of magnitude. Thirdly, the field can be shown to be coherent over distances much larger than the wavelength along the interface. A fact that contradicts the widely accepted point of view that a thermal source of light is incoherent.

The fact that radiative properties of a surface can be tuned by modifying the surface profile has been known for a long time. In particular, the effect of a grating has been studied in great detail [11]. A spectacular effect has been predicted and verified experimentally [25] in 1976 : ruling a shallow sinusoidal grating on a gold surface may lead to a total absorption of a particular polarization. This behaviour has been associated with the resonant excitation of a mode of the surface : a surface plasmon polariton. Due to its resonant character, this absorption takes place for a particular angle once the frequency is fixed. The role of surface plasmons had been observed for a long time as they produced anomalies in the diffraction by gratings.

This type of strong absorption is never observed on flat surfaces. The reason is that the component of the wavevector parallel to the interface is always larger

than ω/c for a surface wave whereas an incident wavevector has a component parallel to the surface given by $\omega/c \sin\theta$. It is thus impossible to have a phase matching of the two waves along the interface. Resonant absorption can take place only if some means is used to fulfil the phase matching condition. When using a periodic modulation of the surface, the diffracted field has components of the form $\omega/c + q2\pi/a$ where a is the period and q is an integer. Note that surface waves ae extensively studied in Appendix B.

The absorption is not the only radiative property that is modified by the surface profile modulation. According to Kirchhoff's law (see Appendix A), the emissivity of a surface is equal to the absorptivity. It is thus expected to observe a peak of emission in a given direction and at a given wavelength provided that Kirchhoff's law is valid for directional polarized quantities. This has been a subject of debate for some time but the question was finally settled [22] when a formal derivation of this result was derived from the reciprocity theorem that follows from Maxwell's equations. Based on this argument, it is thus expected to observe a manifestation of surface wave in the emission of light by surfaces. This has indeed been observed recently by Kreiter et al. [10] on a gold surface heated at $700°C$. To summarize, the mechanism which is involved in such an emission is the following : surface waves are excited by heating the material, then they are diffracted by the grating in directions for which the condition of phase matching is met. This mechanism is reported in Fig. 5

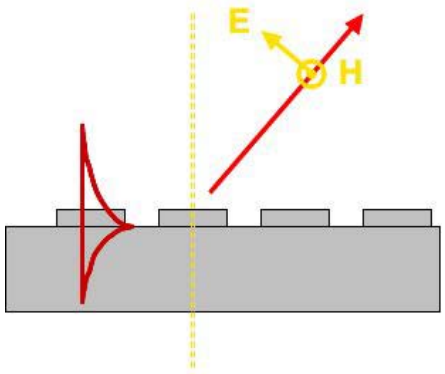

Figure 5: Surface-plasmon assisted emission of radiation. The surface wave is excited by heating the material.

Because of the range of temperature needed, it is easier to observe these effects in the infrared. Although surface plasmon polaritons may exist for highly doped semiconductors, it is easier to observe these phenomena by taking advantage of a different type of surface waves. They are called surface phonon polaritons. They can be viewed schematically as phonons in an ionic crystal. The mechanical vibration of the ions generates a charge oscillation and therefore an electromagnetic wave. We now review the state-of-art of microstructured radiators.

3.2 Review of coherent thermal sources and other microstructured radiators

In the early eighties, Zhizhin *et al.* have studied thermal emission of materials supporting surface phonon polaritons [26]. They worked with a ZnSe crystal sample including periodic inhomogeneities on its surface. The sample was heated at $150°\mathrm{C}$ in order to excite surface waves. Coupling these waves with the periodic profile, they observed emissivity spectra in the p-polarization changing with the direction of observation.

Later on, Hesketh and Zemel measured thermal emission at $400°\mathrm{C}$ of doped silicon gratings. They observed resonances in the emission amplitude in the p-polarization and different spectra when varying the grating period [27–29]. It is only in 2001 that the role of surface waves in thermal emission and its significance in terms of spatial coherence has been highlighted in a paper by Greffet *et al.* [9].

Many other authors have explored experimentally the role of texture on emissivity. We will not mention here the works done on gratings with a period larger than the wavelength so that the geometric optics apply. However, several works have been made since the nineties on thermal emission by microstructures, that is to say structures which have at least one dimension lower than the wavelength. We will distinguish two kinds of thermal sources : on the one hand, directional sources, principally based on surface waves and on the other hand, isotropic sources.

3.2.1 Directional sources

Directional thermal sources involve electromagnetic resonances in the microstructures. These resonances can be related to the existence of surface waves

but other mechanisms can as well be involved (Fabry-Perot resonances, cavity modes).

It is now well known that materials supporting surface waves (surface phonon polariton on polar crystals or surface plasmon polariton on metals and doped semiconductors) can generate coherent thermal emission. By the way, thermal sources like SiC [9, 30], gold [10], tungsten [31, 32] or doped silicon [33–35] can emit thermal radiation in a very directional way for a given wavelength. These sources are lamellar gratings. The periodicity of the grating allows a resonant coupling of surface waves with propagating waves. In this case, surface waves are responsible for coherent thermal emission as discussed in section 3.1. Note that in the plane perpendicular to the lines of the grating, coherent thermal emisison occurs only in *p*-polarization

Another way to produce directional emission is to excite other kind of resonances. One simple way to make directional thermal emission is to use multilayer systems. In such systems, interference conditions yield narrow structures for the electromagnetic field in a single absorbing layer embedded in the structure. Thus it is possible to find resonances for absorption and therefore for emission. These multilayer structures are periodic in one direction, with a cell composed by two nonabsorbing dielectrics with two different thicknesses in the general case. Actually, these systems involve Bragg's reflection. These structures have been studied in the following references : [36–43]. The directional emission is possible in both *p*- or *s*-polarization [41,43]. Note that a few works have been made at the crossing between lamellar gratings and multilayer structures [44]. Here, the electromagnetic resonance is a guided mode in a single layer. The waveguide is surrounded by a lamellar grating which allows the coupling between the field resonance in the guide and propagating waves.

One can design other periodic structures involving other resonances of the electromagnetic field. It is the case of microcavities and photonic crystals. Microcavities can be viewed as 2D-photonic crystals. Thermal radiation by such structures has been experimentally [45, 46] and also numerically [47] studied. Other works have been also made with 3D-photonic crystals. A theoretical and experimental work has been published for multilayer structures in which one layer over two is 2D periodically corrugated [48]. Other works deal with woodpile structures that has been also studied both theoretically and experimentally [49,50]. Sai *et al.*

made also calculations and measurements on a 3D V-grooved silicon grating with an SiO_2 mask layer and interpret their observation in terms of resonance between the field and the grating [51]. Finally, let us mention an attempt to use a photonic crystal structure of tungsten to modify the radiative properties [52]. Note that in 1995, Auslander and Hava have studied anomalous reflectance in doped silicon lamellar gratings due to the surface profile of a grating. Yet, they worked in s-polarization [53]. Nevertheless they noticed in 1998 an antireflective behavior in the p-polarization for V-grooved silicon grating with an SiO_2 mask layer [54]. Such structures could be obviously used in directional thermal emission applications.

3.2.2 Isotropic sources

For cooling applications, isotropic thermal sources are more interesting as we will see in section 4. Therefore, coherent thermal sources are not fully adapted for such applications. However several structures can be used to produce isotropic thermal emission.

By the way, it is always possible to derive isotropic emission from surface waves. It has been shown that using the asymptotic part of the dispersion relation (see Appendix B) of surface waves, one can obtain isotropic emission for a wavelength given by the position of the asymptote. This kind of work has been made with lamellar gratings [30, 34]. Isotropic sources have also been obtained using a coupling between guided modes and surface waves in 2D-periodic metallic structures [55].

On top of that, another possibility to have isotropic thermal sources is to use a well-known anti-reflective system, so called Salisbury screens (see Fig.6). This is an interferometric system coupled to an absorbing thin layer which can be used in detection system [56–58] or in photovoltaic systems [59, 60]. In these systems, there is a broadband and isotropic absorption. By Kirchhoff's law, we can therefore obtain broadband and isotropic thermal emission. Let us introduce quickly the principle of such a system. We note λ_m the wavelength of the maximum of the Planck's function at temperature T. A plane metallic interface behaves as a perfect mirror and we find interferences between the incident and the reflected field. the principle of Salisbury screen is to put a thin absorbing layer on a bright fringe of the inteference pattern. The first bright finge is located at $\lambda/4$ above

the interface. The most simple system is thus composed by a spacer layer (with a thickness $\lambda_m/4$) surrounded by a thin metallic (absorbing) layer. Hence, the system is optimized to be absorbing at λ_m.

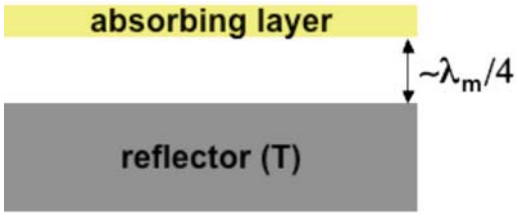

Figure 6: Salisbury screen : an absorbing layer is located at a distance of approximately $\lambda_m/4$, above a reflector, where λ_m is the wavelength of the maximum of the Planck's function at temperature T.

4 Comparison of coherent thermal sources with planar radiators and calculations

Let us now see in what way the microstructured radiators could be interesting for cooling or directional heating applications. Both applications will be studied in the following subsection. All the calculations have been made in *p*-polarization. Similar results could be calculated in *s*-polarization. As we are going to see, the most relevant system for applications such as either radiative cooling or directional heating is Salisbury's screen. This kind of structure does not involve surface waves and is thus less sensitive to the polarization.

4.1 Radiative cooling

The satellite is heated by the radiations emitted from the sun, mainly in the visible region. The temperature of the system increases and the satellite radiates in the infrared range. This emission allows the satellite to be cooled. For efficient radiative cooling, the system will have to be highly emissive in the infrared range, which is equivalent for an opaque material to have a very low reflectance. On the opposite, to avoid the heating of the satellite, the material will have to be very reflective. In this way, the presence of Aluminum on the satellite is a good thing : in the visible range the material acts like a mirror, and few radiation is absorbed. However, metals are good mirrors in the infrared too, so that their emissivity in this spectral range is very low and the radiative cooling unefficient. We propose here to improve this system using a structure which can be an isotropic thermal source. Structures using surface waves have an emissivity which can reach unity but only for a given wavelength [9]. As a result, it has been shown that the best choice is Salisbury's screen [33, 35].

Such a structure is composed by two layers. A non-absorbing dielectric spacer layer with an optical index of about 1.5 and a thin metallic (absorbing) layer. The spacer thickness is of the order of $\lambda_m/4$ in which λ_m is the wavelength of the maximum of Planck's function. As a result, the absorbing layer is on a bright fringe for λ_m, so that there is a maximum for absorption at this wavelength. We calculate λ_m using Wien's law for a body at temperature T. As we wrote in section 3.2.2, the structure will present a spacer layer with a thickness of the order

of $\lambda_m/4$ taking into account the refractive index of the spacer layer. This layer will be surrounded by a thin absorbing layer.

The calculation have been made with silver for this layer but could be made for aluminum as well. Actually, the advantage of silver is to obtain thicknesses greater than for aluminum. Thus a silver film would be technologically more simple to realize. The results that we will see are given for a material at $T = 350°\mathrm{K}$. The maximum of Planck's function for a body at a this temperature is $8.4\ \mu\mathrm{m}$. As a result, the spacer thickness can be numerically optimized: we obtain $2.2\ \mu\mathrm{m}$, and a surrounded layer in silver of 1 nm. The structure has been optimized to have a maximal emissivity. Note that it is possible to shift the peak wavelength increasing the spacer thickness.

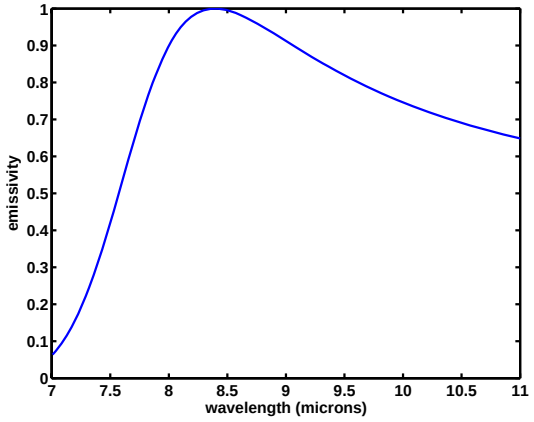

Figure 7: Emissivity spectrum for Salisbuy's screen characterized by a spacer thickness of $2.2\mu\mathrm{m}$, and a silver layer of 1 nm. The direction of observation is normal to the surface.

For this structure, the reflectivity in the visible range is greater than 0.85 : it is a good mirror. It is seen in Fig. 7 that in the infrared range, the emissivity goes to one and is broadband. Thus, it is possible to have a large emissivity in the whole frequency region in which Planck's curve takes significant values.

The next step is to check if the emission is isotropic. In order to calculate this, we have to focus on the integrated emissivity over the whole emission spectrum in each direction. This calculation yields the total emitted power in each direction of

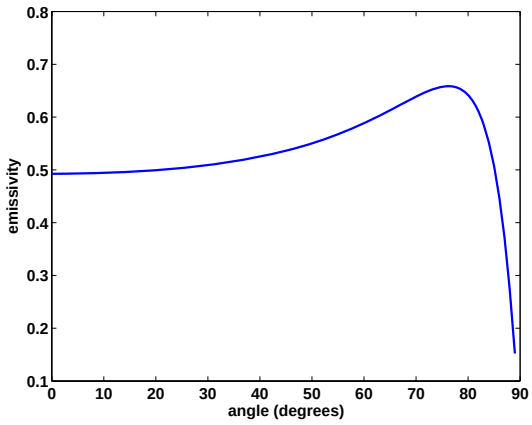

Figure 8: Integrated emissivity over the whole spectrum for Salisbuy's screen characterized by a spacer thickness of $2.2\mu\mathrm{m}$, and a silver layer of 1 nm.

observation. We show the result in Fig. 8. One can see that the emission is uniform over the directions. Emissivity is about 0.5 comparing to the case of aluminum bulk in which the emissivity is always below 0.05 for the same spectral range.

4.2 Directional heating

It is possible to optimize structures for which we have a very directional emission for λ_m. We define λ_m as the wavelength of the maximum of Planck's function. For this application, one can use either lamellar gratings and surface waves or Salisbury's screen. In the case of Salisbury's screen, the radiative properties are less dependant of polarization comparing to lamellar gratings (coupling of surface waves with propagating waves). Therefore it is obvious that in applications like radiative cooling in which we have to integrate over the whole spectrum, every directions and over both polarizations, we must choose Salisbury's screen structures. For directional heating, lamellar gratings present a weak dependance between wavelength and directions. The system is very directional for a given wavelength but becomes more isotropic when integrating over the whole spectrum. As a result, Salisbury's screen is once more the best choice we can make for this application. Hence, this is the only structure we are going to study in this

section. We have to choose a spacer thickness of about $5\lambda_m/4$. We have always a bright fringe at λ_m, and thus maximal absorption. However the condition of phase matching is met for a band spectrum narrower than in the case of radiative cooling.

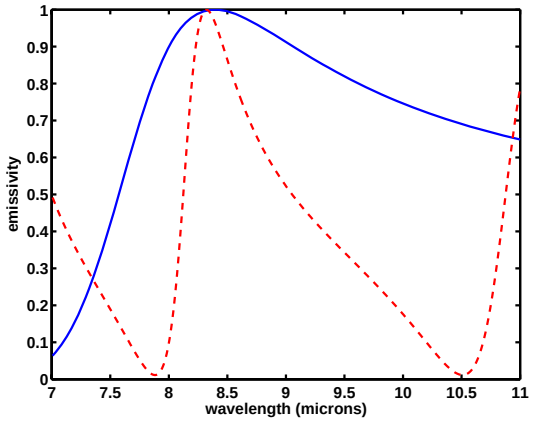

Figure 9: Emissivity spectrum for Salisbuy's screen characterized by a spacer thickness of $10.5\mu\mathrm{m}$, and a silver layer of 1 nm (red dotted line) compared to the calculation of Fig. 7 (blue solid line). The direction of observation is normal to the surface.

We made calculations with a spacer thickness of $10.5\mu\mathrm{m}$, and a silver layer of 1 nm. Results are shown in Fig. 9 and Fig. 10. One can see than this structure is more selective than the previous one both angularly and spectrally. By adding more layers, it is possible to modify both the spectrum and the directivity of the source.

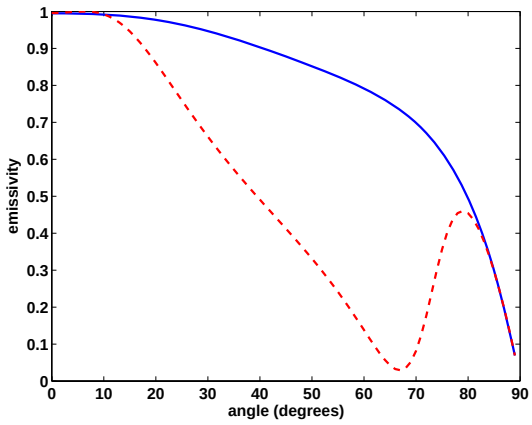

Figure 10: Emissivity angular distribution for Salisbuy's screen characterized by a spacer thickness of 10.5μm, and a silver layer of 1 nm (red dotted line) at $\lambda_m = 8.4\mu$m compared to the same calculation for a spacer thickness of 2.2μm (blue solid line).

5 Scalability and robustness of the microstructured radiators

Once optimized for radiative cooling or directional heating, the microstructured radiators have to be integrated in the satellites. The issues of the scalabity and the robustness to charging and cosmic radiation of the radiators have to be adressed. This is the goal of this part.

5.1 Scalability

As long as the radiator is larger than the coherence length (see Appendix C) of the thermal radiation for directional emission, the radiative properties of the microstructured materials will be unchanged compared to the case of infinite periodic structure.

5.2 Effect of charging and cosmic radiation.

The radiative properties (its emissivity for instance) of a structure are determined by its dielectric constant, magnetic permeability (ϵ_r and μ_r) and the geometry of its interface. Let us consider the effect of charging and cosmic radiation on those parameters.

For any material, the effect of charging is a modification of the surface charges so that it will not have any effect on the dielectric constant nor on the performance of the microstructured radiators.

The effect of cosmic radiation is more complicated and has to be analyzed in details. Let us first consider the effect of solar wind which is the main radiation impinging on the satellites. This solar wind is composed of 95% of protons with average energy of 1keV (corresponding to a mean velocity of 450 km/s) and with an incident flux of 1.35×10^{12} protons/m^2/s. We need to investigate the kind of damages on the structure of aluminium (material of the radiators we are interested in) which could lead to a change in its optical properties.

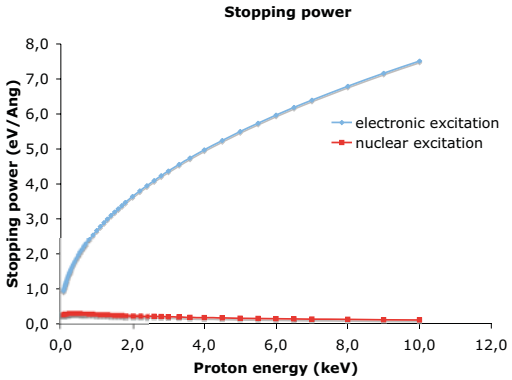

Figure 11: Stopping power in eV per Angstrom

Thanks to a MonteCarlo calculation, we have simulated the effect of protons of a given energy incident on a substrate of Al. We have access separately to the

energy per unit length that the protons give to the electrons, and to the energy given to the nuclei. This power loss per unit length is called the stopping power. Figure 11 summarizes the stopping power obtained for incident protons of energy range [0.1,10 keV]. First, we see that a major part of the energy of the protons is given to the electrons, as the stopping power for electrons is 10 times larger than the stopping power of the nuclei. The maximum of the stopping power due to electronic excitation is approximately of 7 eV per Å. This value is far below the threshold where damages occur to the structure of the materials (typically several keV per nm) [61,62]. The collisions with the nuclei could give rise to the creation of Frenkel pairs (interstitial-vacancy pair). The radiators being at a temperature of 200^oC, these pairs will recombine leaving no defects in the structure of Al.

Finally, we have to analyze the penetration of the protons inside the structure and what happens with the excess of protons. Fig. 12 shows the penetration depth versus the energy of the incident protons. For an energy of 1keV, the penetration length is of 158 Å.

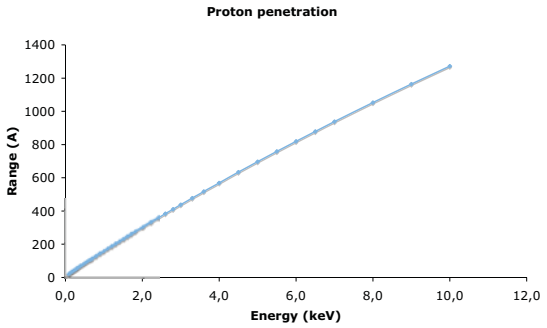

Figure 12: Penetration depth (range in Å), versus the energy of the protons impinging on the substrate.

The remaining question is to know what effects are caused by the excess of protons inside the aluminium. Unfortunately, we have verified that those protons were not backscattered but implanted into the material.

Due to diffusion inside the metal, the protons will either diffuse to the surface and be evacuated as dihydrogen, or to inside of the materials causing a mechanical fragilisation of the materials. The impact on the dielectric constant is not obvious since the damage will only affect a small region (150 Å) near the surface. This effect will also very much depend on the surface of the radiators although expected to be negligible.

In conclusion, we expect that the integration of the microstructured radiators on the satellites will not lead to a significant modification of its radiative properties compared to those predicted by the calculations made with the parameters taken in normal conditions of pression and temperature on Earth. The effect of charging is clearly negligible. The effect of cosmic radiation is expected to be negligible but further studies should be made to ensure that the implantation of protons inside the radiators will not damage the structure.

6 Conclusion

This report offers a complete review about the modification of the radiative properties of microstructured radiators. We have first reviewed the three different mechanisms responsible for an enhancement of the emissivity. Chapter 3 gives the state-of-art of microstructured radiators. In particular, the phenomenon of coherent thermal emission has been explained in details. Coherent thermal emission from lamellar gratings is very sensible to polarization. Hence, Salisbury's screen has been shown to present a better choice for both radiative cooling and directional heating. Comparison of the efficiency of Salisbury's screen with planar radiators has been proposed in Chapter 4. An enhancement of the emissivity of more than 90% compared to the plane radiator has been demonstrated. The key issue of scalability and robustness of such microstructured radiators is treated in Chapter 5. We have shown than the effect of charging was negligible. We expect that the effect of cosmic radiation will be negligible as well. Nevertheless, we think that further studies will be needed to estimate more quantitatively the impact of protons implantations in the radiators.

A Basic concepts in radiometry and fundamentals limits of thermal sources

A.1 Basic definitions

The basic concept of radiometry is the specific intensity $I_\nu(\mathbf{r}, \mathbf{s})$ used to describe the energy flux through a surface element dA with normal $\mathbf{n}$ around a point of coordinates $\mathbf{r}$ propagating in the direction specified by the unit vector $\mathbf{s}$. The flux of energy flowing through dA in the interval of frequencies $[\nu, \nu + d\nu]$ can be written as

$$dQ_\nu = I_\nu(\mathbf{r}, \mathbf{s}) dA \cos\theta d\Omega, \tag{7}$$

where $\cos\theta = \mathbf{n} \cdot \mathbf{r}$. Note that when dealing with planar sources, the specific intensity emitted by the source is often refered to as radiance. The flux of energy per solid angle integrated over a surface (e.g. the area of the source or the area of a scattering surface illuminated by a finite beam) is given by the radiant intensity $J_\nu(\mathbf{s})$:

$$J_\nu(\mathbf{s}) = \int I_\nu(\mathbf{r}, \mathbf{s}) \cos\theta dA. \tag{8}$$

The bidirectional reflection distribution function $\rho_\nu(\mathbf{r}, \mathbf{s}, \mathbf{s})$ (BRDF) expresses the contribution that the incident specific intensity $I_\nu^{inc}(\mathbf{r}, \mathbf{s}')$ makes to the reflected specific intensity $I_\nu^r(\mathbf{r}, \mathbf{s}')$ in the direction $\mathbf{s}$. It is defined as

$$I_\nu^r(\mathbf{r}, \mathbf{s}) = \int \rho(\mathbf{r}, \mathbf{s}, \mathbf{s}') I_\nu^{inc}(\mathbf{r}, \mathbf{s}') \cos\theta' d\Omega'. \tag{9}$$

Note that this definition implies that the link between the incident and reflected specific intensities is local and depends on $\mathbf{r}$. An expression of the BRDF can be derived in an electromagnetic framework as shown in Ref. [22]. In particular, it can be proved that $\rho(\mathbf{r}, \mathbf{s}, \mathbf{s}') = \rho(\mathbf{r}, -\mathbf{s}', -\mathbf{s})$, a property that is a consequence of the reciprocity of Maxwell equations. In simple words, when using a point-like source and a point-like detector, one gets when the same signal upon interchanging source and detector. This property is valid provided that all the materials are described by dielectric and magnetic symmetric tensors.

A.2 Kirchhoff's law. A bound for the emissivity.

An interesting consequence of the reciprocity of the BRDF is that it allows to obtain Kirchhoff's law which states that the emissivity is equal to the absorptivity. From this statement, it follows that the emissivity is always smaller than 1. In other words, a source cannot emit more than the blackbody specific intensity. Several derivations are based on thermodynamic balances. However, they cannot be applied to surfaces that reflect non-specularly. Because this property has been overlooked in some recent works, we repeat its derivation here for the sake of completeness.

At thermodynamic equilibrium, the specific intensity I_ν^o is both isotropic and homogeneous, and it only depends on temperature T. On the other hand, the thermal emission of a body at this temperature is described by the emitted specific intensity I_ν^e. This quantity is characterized by the directional spectral emissivity $\epsilon_\nu(\mathbf{r}, \mathbf{s})$ defined by:

$$I_\nu^e(\mathbf{r}, \mathbf{s}) = \epsilon_\nu(\mathbf{r}, \mathbf{s}) I_\nu^o(T). \tag{10}$$

In order to establish a connection between the reflectivity and the emissivity, we assume that the surface is contained in a medium at thermodynamic equilibrium. Hence, the specific intensity is at any point the equilibrium specific intensity $I_\nu^o(T)$. At points close to the surface, we can express that the specific intensity is either emitted or reflected by the surface according to the expression:

$$I_\nu(T) = \epsilon_\nu(\mathbf{r}, \mathbf{s}) I_\nu^o(T) + \int \rho_\nu(\mathbf{r}, \mathbf{s}, \mathbf{s}') I_\nu^o(\mathbf{r}, \mathbf{s}') \cos\theta' d\Omega'. \tag{11}$$

We have used the fact that the incident radiation is the equilibrium radiation. The angular integration is carried out over a hemisphere with $\cos\theta' < 0$. Therefore, from Eq. (11), we obtain:

$$1 = \epsilon_\nu(\mathbf{r}, \mathbf{s}) + \int \rho_\nu(\mathbf{r}, \mathbf{s}, \mathbf{s}') \cos\theta' d\Omega' = \epsilon_\nu(\mathbf{r}, \mathbf{s}) + \rho_\nu(\mathbf{r}, \mathbf{s}, h) \tag{12}$$

In Eq. (12) the notation $\rho_\nu(\mathbf{r}, \mathbf{s}, h)$ has been introduced for the BRDF integrated over all angles of incidence characterized by $\mathbf{s}'$. This quantity is called hemispherical directional reflectivity.

On the other hand, let us now consider a field illuminating an opaque surface. Then, its energy is either reflected or absorbed. The conservation of energy gives the following relation :

$$1 = \alpha_\nu(\mathbf{r}, \mathbf{s}) + \int \rho_\nu(\mathbf{r}, \mathbf{s}', \mathbf{s}) \cos\theta' d\Omega' = \alpha_\nu(\mathbf{r}, \mathbf{s}) + \rho_\nu(\mathbf{r}, h, \mathbf{s}) \qquad (13)$$

In Eq. (13), the BRDF is integrated over the hemisphere with $\cos\theta' > 0$ of reflected angles, $\alpha_\nu(\mathbf{r}, \mathbf{s})$ represents the spectral directional absorptivity and $\rho_\nu(\mathbf{r}, h, \mathbf{s})$ is called directional hemispherical reflectivity. On comparing Eq. (12) and (13), we see that the spectral directional emissivity is equal to the spectral directional absorptivity provided that

$$\rho_\nu(\mathbf{r}, h, \mathbf{s}) = \rho_\nu(\mathbf{r}, \mathbf{s}, h). \qquad (14)$$

The equality (14) follows immediately from the reciprocity relation derived in Ref. [22]. Thus, Eq. (14) shows that the reciprocity entails that the emissivity is equal to the absorptivity. This result is known as Kirchhoff's law. It proves that a thermal source has a fundamental limit : it cannot emit in free space more than a blackbody. *In other words, the emissivity is always smaller than 1*. By modifying the interface of a planar source, the angular emission pattern can be modified, the value of the emissivity can be increased up to 1 but it is not possible to go beyond 1.

Note however that more power can be extracted from a source by bringing matter in the near field of a source. This is discussed at length in Ref. [63].

B Introduction to surface electromagnetic waves

In this section, we give a brief introduction to the main properties of electromagnetic surface waves. This particular type of waves exists at the interface between two different media. An electromagnetic surface wave propagates along the interface and decreases exponentially in the perpendicular direction. Surface waves due to a coupling between the electromagnetic field and a resonant polarization oscillation in the material are called surface polaritons. From a microscopic point of view, the surface waves at the interface of a metal is a charge density wave or plasmon. It is therefore called surface-plasmon polariton. At the interface of a dielectric, the surface wave is due to the coupling of an optical phonon with the electromagnetic field. It is thus called surface-phonon polariton. Plasmon polaritons and phonon polaritons can also exist in the whole volume of the material and are called polaritons. More details about this subject can be found in textbooks such as Kittel [64], Ashcroft and Mermin [65] and Ziman [66]. In what follows, we will focus our attention on surface polaritons propagating along a plane interface. Excellent reviews of the subject can be found in [67–70].

B.1 Surface polaritons

Let us now study the existence and the behaviour of surface polaritons in the case of a plane interface separating two linear, homogeneous and isotropic media with different dielectric constants. The system considered is depicted in Fig.13.

The medium 1 (dielectric constant $\epsilon_1(\omega)$ and magnetic constant $\mu_1(\omega)$) fills the upper half-space $z > 0$ whereas medium 2 (dielectric constant $\epsilon_2(\omega)$ and magnetic constant $\mu_2(\omega)$) fills the lower half-space $z < 0$. The two media are supposed to be local and dispersive so that their complex dielectric and magnetic constants only depend on ω.

The three directions x, y, z shown in Fig.13 are characterized by their unit vectors $\hat{\mathbf{x}}, \hat{\mathbf{y}}, \hat{\mathbf{z}}$. A point in space will be denoted $\mathbf{r} = (x, y, z) = x\hat{\mathbf{x}} + y\hat{\mathbf{y}} + z\hat{\mathbf{z}} = (\mathbf{R}, z)$ where $\mathbf{R} = x\hat{\mathbf{x}} + y\hat{\mathbf{y}}$. Similarly, a wave vector $\mathbf{k} = (k_x, k_y, k_z)$ will be denoted by $\mathbf{k} = (\mathbf{K}, \gamma)$ where $\mathbf{K}$ is the component parallel to the interface and $\gamma = k_z$ the component in the z direction.

A surface wave is a particular solution of Maxwell's equations which propagates along the interface and decreases exponentially in the perpendicular direc-

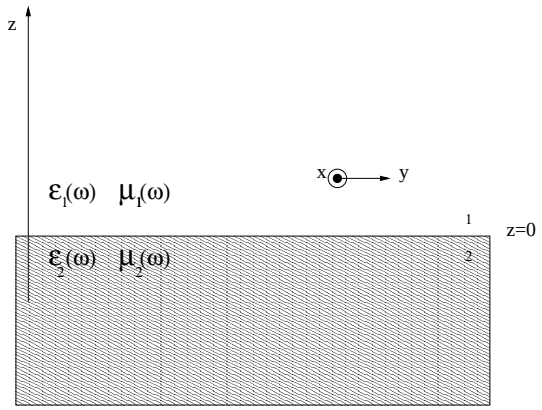

Figure 13: A plane interface separating medium 1 (dielectric constant $\epsilon_1(\omega)$, magnetic constant $\mu_1(\omega)$) and medium 2 (dielectric constant $\epsilon_2(\omega)$, magnetic constant $\mu_2(\omega)$)

tions. Because of the translational invariance of the system, it can be cast in the form:

$$\mathbf{E}_1(\mathbf{r},\omega) = \begin{pmatrix} E_{x,1} \\ E_{y,1} \\ E_{z,1} \end{pmatrix} \exp[i(\mathbf{K}.\mathbf{R} + \gamma_1 z)] \text{ (Medium1)}, \tag{15}$$

$$\mathbf{E}_2(\mathbf{r},\omega) = \begin{pmatrix} E_{x,2} \\ E_{y,2} \\ E_{z,2} \end{pmatrix} \exp[i(\mathbf{K}.\mathbf{R} - \gamma_2 z)] \text{ (Medium2)}, \tag{16}$$

where γ_1 and γ_2 are given by,

$$\gamma_1^2 = \epsilon_1(\omega)\mu_1(\omega)k_0^2 - K^2 \quad \text{with } Im(\gamma_1) > 0, \tag{17}$$

$$\gamma_2^2 = \epsilon_2(\omega)\mu_2(\omega)k_0^2 - K^2 \quad \text{with } Im(\gamma_2) > 0. \tag{18}$$

Here $k_0 = \omega/c$ where c is the speed of light in vacuum. We now look for the existence of surface waves in s (TE) or p (TM) polarization. In what follows, we shall assume that the wave propagates along the y-axis.

B.1.1 s-polarization (TE)

In s-polarisation, the electric field is perpendicular to the plane (y, z). The electric field $\mathbf{E}$ is thus parallel to the x direction

$$\mathbf{E}_1(\mathbf{r}, \omega) = E_{x_1}\hat{\mathbf{x}} \exp[i(\mathbf{K}.\mathbf{R} + \gamma_1 z)], \tag{19}$$

$$\mathbf{E}_2(\mathbf{r}, \omega) = E_{x_2}\hat{\mathbf{x}} \exp[i(\mathbf{K}.\mathbf{R} - \gamma_2 z)]. \tag{20}$$

The magnetic field is then derived from the Maxwell equation $\mathbf{H} = -i\nabla \times \mathbf{E}/(\mu(\omega)\omega)$. The continuity conditions of the parallel components of the fields across the interface yield the following equations :

$$E_{x,1} - E_{x,2} = 0, \tag{21}$$

$$\frac{\gamma_1}{\mu_1(\omega)}E_{x,1} + \frac{\gamma_2}{\mu_2(\omega)}E_{x,2} = 0. \tag{22}$$

We search a mode of the system which is a solution of the homogeneous problem. The system has a non-trivial solution if and only if

$$\mu_2(\omega)\gamma_1 + \mu_1(\omega)\gamma_2 = 0. \tag{23}$$

Taking into account equations (17,18), one obtains from (23) the surface wave dispersion relation for s-polarization:

$$K^2 = \frac{\omega^2}{c^2}\frac{\mu_1(\omega)\mu_2(\omega)[\mu_2(\omega)\epsilon_1 - \mu_1(\omega)\epsilon_2]}{\mu_2^2(\omega) - \mu_1^2(\omega)}. \tag{24}$$

For the particular case where $\epsilon_1 = \epsilon_2$, the dispersion relation takes the simple form:

$$K^2 = \frac{\omega^2}{c^2}\frac{\mu_1(\omega)\mu_2(\omega)}{\mu_1(\omega) + \mu_2(\omega)}. \tag{25}$$

B.1.2 p-polarization (TM)

For p-polarization, the electric field lies in the plane (y, z) and can be cast in the form:

$$\mathbf{E}_1(\mathbf{r}, \omega) = \begin{pmatrix} 0 \\ E_{y,1} \\ E_{z,1} \end{pmatrix} \exp[i(\mathbf{K}.\mathbf{R} + \gamma_1 z)], \tag{26}$$

$$\mathbf{E}_2(\mathbf{r},\omega) = \begin{pmatrix} 0 \\ E_{y,2} \\ E_{z,2} \end{pmatrix} \exp[i(\mathbf{K}.\mathbf{R} - \gamma_2 z)]. \tag{27}$$

The continuity of the tangential electric field yields

$$E_{y,1} - E_{y,2} = 0. \tag{28}$$

The Maxwell equation $\nabla.\mathbf{E} = 0$ imposes a relation between the two components of the electric field

$$KE_{y,2} - \gamma_2 E_{z,2} = KE_{y,1} + \gamma_1 E_{z,1} = 0. \tag{29}$$

The continuity of the z-component of D yields:

$$\epsilon_1(\omega)E_{z,1} = \epsilon_2(\omega)E_{z,2}. \tag{30}$$

Inserting (30) and (28) in (29) yields

$$\epsilon_1(\omega)\gamma_2 + \epsilon_2(\omega)\gamma_1 = 0. \tag{31}$$

Using (17) and (18), we obtain the surface wave dispersion relation for *p*-polarization and non-magnetic media

$$K^2 = \frac{\omega^2}{c^2}\frac{\epsilon_1(\omega)\epsilon_2(\omega)}{\epsilon_1(\omega) + \epsilon_2(\omega)}. \tag{32}$$

B.1.3 Remarks

- When the media are non-magnetic, there are no surface waves in s-polarization. Indeed, the imaginary part of the z-components γ_i is always positive, so that $\gamma_1 + \gamma_2$ cannot be zero.
- At a material-vacuum interface ($\epsilon_1(\omega) = \mu_1(\omega) = 1$), the dispersion relation reads in p-polarization

  $$K = \frac{\omega}{c}\sqrt{\frac{\epsilon_2(\omega)}{\epsilon_2(\omega) + 1}}. \tag{33}$$

  It follows that the wave vector becomes very large for a frequency such that $\epsilon(\omega) + 1 = 0$.

- The conditions (23) and (31) corresponds to the poles of the Fresnel reflection factors. To search these poles is an alternative and simple way to find the dispersion relation. This is particularly useful when searching the dispersion relation for multilayers system.

- For non-lossy media, one can find a real K corresponding to a real ω. This mode exists only if $\epsilon_2(\omega) < -1$ in the case of an interface separating a vacuum from a material.

- In the presence of losses, the dispersion relation yields two equations but both frequency and wavector can be complex so that there are four parameters. Two cases are of practical interest : i) a real frequency and a complex wavevector, ii) a complex frequency and a real wavector. These two choices leads to different shapes of the dispersion relation as discussed in [8,71–73]. The imaginary part of ω describes the finite lifetime of the mode due to losses. Conversely, for a given real ω, the imaginary part of K yields a finite propagation length along the interface.

- The dispersion relation (33) shows that for a real dielectric constant $\epsilon_1(\omega) < -1$, $K > \omega/c$. This mode cannot be excited by a plane wave whose wavevector is such that $K < \omega/c$. In order to excite this mode, it is necessary to increase the wavevector. One can use a prism [67, 74, 75] or a grating [8]. A scatterer can also generate a wave with the required wavevector.

B.2 Dispersion relation

In this subsection, we will consider two types of surface waves: surface-plasmon polaritons and surface-phonon polaritons. Surface-plasmon polaritons are observed at surfaces separating a dielectric from a medium with a gas of free electrons such as a metal or a doped semiconductor. The dielectric constant of the latter can be modelled by a Drude model :

$$\epsilon(\omega) = \epsilon_\infty - \frac{\omega_p^2}{\omega^2 + i\Gamma\omega}, \tag{34}$$

where ω_p is the plasma frequency and Γ accounts for the losses. Using this model and neglecting the losses, we find that the resonance condition $\epsilon(\omega) + 1 = 0$

yields $\omega = \omega_p/\sqrt{2}$. For most metals, this frequency lies in the near UV so that these surface waves are more difficult to excite thermally. By contrast, surface-phonon polaritons can be excited thermally because they exist in the infrared. They have been studied through measurements of emission and reflectivity spectra by Zhizhin and Vinogradov [76]. Let us study the dispersion relation of surface-phonon polaritons at a vacuum/Silicon Carbide (SiC) interface. SiC is a non-magnetic material whose dielectric constant is well described by an oscillator model in the [2-22 μm] range [77]:

$$\epsilon(\omega) = \epsilon_\infty \left(1 + \frac{\omega_L^2 - \omega_T^2}{\omega_T^2 - \omega^2 - i\Gamma\omega}\right), \tag{35}$$

with $\omega_L = 969$ cm^{-1}, $\omega_T = 793$ cm^{-1}, $\Gamma = 4.76$ cm^{-1} and $\epsilon_\infty = 6.7$. The dispersion relation at a SiC/vacuum interface is represented in Fig. 14.

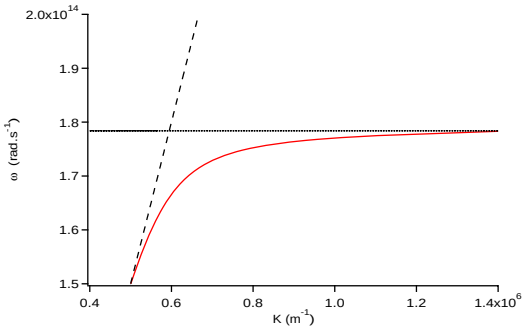

Figure 14: Dispersion relation for surface phonon-polariton at a SiC/Vacuum interface. The flat asymptote is situated at $\omega_{asym} = 1.784\ 10^{14}$ rad s^{-1}. The slanting dashed line represents the light cone above which a wave is propagating and below which a wave is evanescent.

This dispersion relation has been derived by assuming that the frequency ω is complex and the parallel wavevector K is real. This choice is well suited to analyse experimental measurements of spectra for fixed angles. The width of the resonance peaks observed is related to the imaginary part of the frequency of the mode. We note that the curve is situated below the light cone $\omega = cK$ so that the surface wave is evanescent. We also observe a horizontal asymptote for $\omega_{asym} = 1.784\ 10^{14}$ rad s^{-1} so that there is a peak in the density of electromagnetic

states. In Fig. 15, we have shown the dispersion relation obtained when choosing a real frequency ω and a complex wavevector K. The real part of the complex wavevector is represented. It is seen that the shape of the dispersion relation is significantly changed. A backbending of the curve is observed. This type of behaviour is observed experimentally when performing measurements at a fixed frequency and varying the angle. Observed resonances in reflection or emission experiments have an angular width which is related to the imaginary part of the complex wavevector.

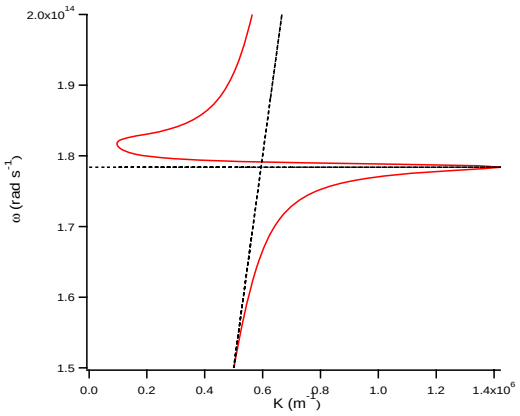

Figure 15: Dispersion relation for surface phonon-polariton at a SiC/Vacuum interface. Real ω chosen to obtain a complex K. The real part of K is represented. The horizontal asymptote is situated at $\omega_{asym} = 1.784\ 10^{14}$ rad s^{-1}. The slanting dashed line represents the light line above which a wave is propagating and below which a wave is evanescent.

We have plotted in Fig.16 the surface wave decay length in the direction perpendicular to the interface versus the wavelength. From Eqs (15) and (16), it is seen that the amplitude of the electromagnetic field decreases exponentially in the z direction with a decay length $\delta_1 = 1/Im(\gamma_1)$ in medium 1 and $\delta_2 = 1/Im(\gamma_2)$ in medium 2.

We note that the smallest penetration depth in SiC is obtained for the frequency ω_{asym}. At this frequency, losses are very large.

We study in Fig. 17 the surface wave propagation length along a SiC-vacuum interface. It is given by the inverse of the imaginary part of the parallel wavevector

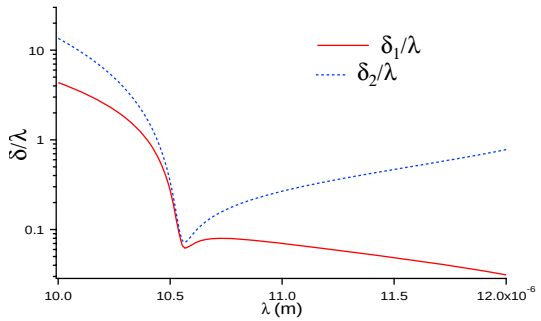

Figure 16: Surface wave decay length along the z-direction in medium 1 and 2 versus the wavelength for a SiC-vacuum interface.

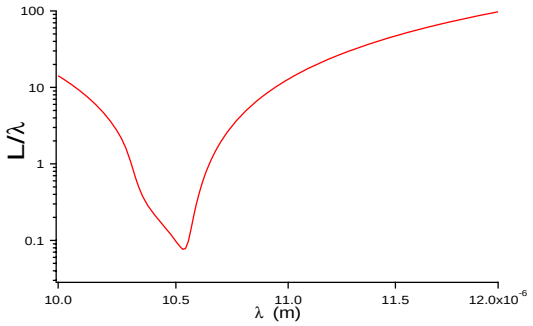

Figure 17: Surface wave propagation length along the interface versus the wavelength λ.

$L = 1/Im(K)$. Around ω_{asym}, L is minimum. It can be as large as several tens of wavelengths.

It will be seen below that the existence of these surface modes is responsible for a long coherence time and a long coherence length of the electromagnetic field in the near field. They are essentially given by the lifetime and the decay length of the surface wave.

C Basic concepts in coherence theory

C.1 Temporal and spatial coherence

The concept of coherence of electromagnetic fields is fundamentally related to the randomness of light. Radiation of a thermal source is due to the radiation produced by the random motion of charges. A laser electromagnetic field has also some randomness due to the random phase of spontaneous emission. Thus any electromagnetic field must be described within a statistical framework to account for its fluctuations. When dealing with stochastic processes, it is necessary to introduce a probability density that the field takes a given value at a given time and a given point. As far as interferences are concerned, coherence of the field can be characterized by a two-point, two-time correlation function

$$\langle E(\mathbf{r}_1, t_1) E(\mathbf{r}_2, t_2) \rangle.$$

In the above equation, the brackets indicate an ensemble (or statistical) average. This is called a second order coherence function because it involves two fields. For the sake of simplicity, we do not consider the vectorial nature of the electromagnetic fields. The simplest way to test the coherence of a field is to produce interferences. We will show that the description of an interference experiment requires the correlation function. When illuminating two pinholes in an opaque screen at points $\mathbf{r}_1$ and $\mathbf{r}_2$, two diffracted fields are produced. We can look at their interference at a point M located at a same distance $r = c\tau$ from both pinholes. The fields at M can be cast in the form $K_1 E_M(\mathbf{r}_1, t_1 - \tau)$ and $K_2 E_M(\mathbf{r}_2, t_2 - \tau)$. Since an optical detector is sensitive to the intensity, it appears that the intensity at M is the sum of the two intensities produced by each pinhole plus a crossed (or interference) term $2\langle E_M(\mathbf{r}_1, t - \tau) E_M(\mathbf{r}_2, t - \tau) \rangle$. It is seen that this term is exactly the spatial correlation function that characterizes the field at the same time and at two different points. In optics, this correlation of the field at two different points is called spatial coherence [78]. Note that if the correlation were zero, the detector signal would just be the incoherent sum of the two intensities and no interference fringes would be observed. The contrast of the fringes is directly related to the amplitude of the correlation function.

Conversely, one may be interested in studying the time correlation function at the same point and at two different times.This characterizes the *temporal coher-*

ence. It can be said that this function characterizes the memory of the random field. A Michelson interferometer illuminated by a point-like source enables to measure this correlation function. Indeed, two fields following two paths with different lengths and recombining at the detector located at point M yield a signal proportional to the sum of intensities plus an interference term of the form

$$\langle E_M(\mathbf{r}_1, t-\tau_1) E_M(\mathbf{r}_1, t-\tau_2)\rangle.$$

C.2 Coherence and spectral width

We now discuss the link between coherence and spectrum of the source. We start discussing the temporal behaviour. The coherence time τ which is defined as the typical time over which the correlation function $\langle E_M(\mathbf{r}_1, t-\tau_1) E_M(\mathbf{r}_1, t-\tau_2)\rangle$ does not vanish is related to the spectral width $\Delta\nu$ of the radiation by the relation $\Delta\nu\tau \approx 1$. This property follows from the Wiener-Khinchin theorem [78] that states that the correlation function of a stationary process is the Fourier transform of its power spectral density. Hence, the coherence time can always be increased by decreasing the bandwidth of the signal, i.e. by filtering.

There is an equivalent property for spatial coherence. The spatial transverse coherence length Δx perpendicular to a beam is related to the width of the wavevector distribution Δk_x in the angular spectrum of the beam by $\Delta x \Delta k_x \approx 2\pi$. The coherence length can be increased by collimating a beam. Thus a laser pointer is both spatially coherent (highly collimated) and temporally coherent (quasi-monochromatic). Instead, black body radiation is spatially incoherent (isotropic) and temporally incoherent (broad spectrum).

C.3 Spatial coherence and directivity

In what follows, we will show that a narrow angular emission lobe is a signature of the spatial coherence of the field in the plane of the source.

We first introduce an analogue of the Wiener Khinchin theorem (WKT) to analyse the spatial coherence of the field. In simple terms, WKT states that a quasi monochromatic source with bandwidth $\Delta\nu$ has a coherence time roughly equal to $1/\Delta\nu$. Similarly, a quasi parallel beam with a spatial frequency bandwidth Δk_x has a transverse coherence length $2\pi/\Delta k_x$. A formal proof is based

on two properties : the relationship between the cross-spectral density of the field in the plane of the source $z = 0$ and the power spectral density of the field, the relationship between the power radiated in far field and the power spectral density. For a translationally invariant system, the Fourier transform of the field does not converge in the sense of a function. Yet, one can define a field equal to the random field in a square of area A and null outside. We can now define the Fourier transform of the field in the plane $z = 0$ as :

$$\mathbf{E}_A(\mathbf{r}_\parallel, \omega) = \int \frac{d^2\mathbf{K}}{4\pi^2} \, \mathbf{E}_A(\mathbf{K}, \omega) \exp(i\mathbf{K} \cdot \mathbf{r}_\parallel) \tag{36}$$

It can be shown [78] that the WKT yields a relation between the cross-spectral density and the power spectral density of the spectrum of the field :

$$\left\langle E_l(\mathbf{r}_\parallel, \omega) E_l^*(\mathbf{r}_\parallel + \mathbf{r}'_\parallel, \omega) \right\rangle = \int \frac{d^2\mathbf{K}}{4\pi^2} \lim_{A\to\infty} \frac{1}{A} \left\langle E_{l,A}(\mathbf{K}, \omega) E_{l,A}^*(\mathbf{K}, \omega) \right\rangle \exp(i\mathbf{K}\cdot\mathbf{r}'_\parallel), \tag{37}$$

where E_l is a component of the electric field. This relation implies that if the spectrum has a bandwidth smaller than $2\pi/\lambda$, the coherence length is larger than λ. The second step is to show that the bandwidth of the spectrum power density $\left\langle \mathbf{E}_{l,A}(\mathbf{K}, \omega) \mathbf{E}_{l,A}^*(\mathbf{K}, \omega) \right\rangle / A$ is given by the emission pattern in the far field. Indeed, the field can be written everywhere as [5] :

$$\mathbf{E}_A(\mathbf{r}, \omega) = \int \frac{d^2\mathbf{K}}{4\pi^2} \, \mathbf{E}_A(\mathbf{k}, \omega) \exp(i\mathbf{K} \cdot \mathbf{r}_\parallel + i\gamma z), \tag{38}$$

where $\mathbf{k} = (\mathbf{K}, \gamma)$ and γ is given by $\gamma^2 = k_0^2 - \mathbf{K}^2$. This field can be evaluated asymptotically in the far field using the stationary phase approximation [5]. It can be cast in the form :

$$\mathbf{E}_A(\mathbf{r}, \omega) = \frac{K \exp(ikr)}{r} \, \mathbf{E}_A\left(\mathbf{K} = \frac{2\pi}{\lambda}\hat{\mathbf{r}}_\parallel, \omega\right), \tag{39}$$

where K is a constant. The power dP flowing through an element of surface $dS = r^2 d\Omega$ is given by the flux of the Poynting vector. In far field, the Poynting vector has locally a plane wave structure so that its time averaged amplitude is given by $\epsilon_0 c|\mathbf{E}|^2/2$.

$$dP = \frac{\epsilon_0 c}{2} |K|^2 \left| \mathbf{E}_A\left(\mathbf{K} = \frac{2\pi}{\lambda}\hat{\mathbf{r}}_\parallel, \omega\right) \right|^2 d\Omega \tag{40}$$

where $\hat{\mathbf{r}}$ is the unit vector $\mathbf{r}/|\mathbf{r}|$. It appears clearly that the far field pattern is given by the power spectral density of the field. This completes the discussion of the link between the directivity of the emitted field and the coherence of the field in the plane of the source. It is clear that a directional source implies a narrow spectrum and therefore a large correlation length.

C.4 Thermal radiation, coherence and laser radiation

We have argued that thermal radiation can become highly partially coherent by filtering. One may use a quasimonochromatic filter to enhance temporal coherence. One may also use a beam expander with a pinhole at the focal point of the afocal system to increase the spatial coherence. Any system that selects a few subset of propagation directions can be used to this aim. It is therefore fair to ask what is the difference with a laser. The key difference is that after filtering thermal light to increase its coherence, one is left with a very small intensity. Most photons have been discarded. What is specific of a laser is that all the power of the source goes in essentially one single mode. The mean number of photons per mode is given by Bose-Einstein distribution for thermal light and this is much smaller than 1 usually. By contrast, it is much larger than 1 for a laser.

References

[1] S. M. Rytov, Y. A. Kravtsov and V. I. Tatarskii, *Principles of Statistical Radiophysics* (Springer-Verlag, Berlin, 1989).

[2] R. Carminati and J.-J. Greffet, Phys. Rev. Lett. **82**, 1660 (1999).

[3] A.V. Shchegrov, K. Joulain, R. Carminati and J-J. Greffet, Phys. Rev. Lett. **85**, 1548 (2000).

[4] C. Henkel, K. Joulain, R. Carminati and J.J. Greffet. Opt.Commun. **186**, 57 (2000).

[5] L. Mandel and E. Wolf, *Optical coherence and quantum optics* (Cambridge University Press, Cambridge, 1995)

[6] C. Henkel, K. Joulain, J.P. Mulet, J.J. Greffet, Phys.Rev.A, **69**, 023808 (2004).

[7] K. Joulain, Remi Carminati, Jean-Philippe Mulet, Jean-Jacques Greffet, Phys.Rev.B **68**, 245405 (2003).

[8] J. Le Gall, M. Olivier and J.J. Greffet, Phys.Rev.B **55** 10105 (1997).

[9] J.J. Greffet, R. Carminati, K.Joulain, J.P. Mulet, S. Mainguy and Y. Chen, Nature (London) **416**, 61 (2002).

[10] M. Kreiter *et al.*, Opt. Commun. **168**, 117 (1999).

[11] R. Petit, *Electromagnetic theory of gratings* (Springer Verlag, Berlin, 1980).

[12] P. Lalanne and G.M. Morris, J. Opt. Soc. Am.A **13** 779 (1996).

[13] L.Li, *J.Opt.Soc.Am.A* **13** 1024 (1996).

[14] N. Chateau and J.-P. Hugonin, J. Opt. Soc. Am. A **11**, 1321 (1994).

[15] R. Bouchitté and R. Petit, *Electromagnetics* **5** 17 (1985).

[16] P. Lalanne, *Journal of Modern Optics* **43** 2063 (1996).

[17] T.K. Gaylord, E.N. Glytsis, M.G. Moharam *Appl.Opt.* **26** 3123 (1987).

[18] J.Lekner *Theory of reflection* (Dordrecht,Nijhoff, 1987).

[19] W.H. Southwell, Opt. Lett. **8** 584 (1983).

[20] W.H. Southwell, J.Opt.Soc.Am.A **8** 549 (1991).

[21] D. Maystre, O. Mata-Mendez and A. Roger, Opt. Acta **30**, 1707 (1983)

[22] J.-J. Greffet and M. Nieto-Vesperinas, J. Opt. Soc. Am. A **15**, 2735 (1998).

[23] R. Siegel and J. R. Howell, *Thermal Radiation Heat Transfer* (Hemisphere, Washington, D.C., 1981).

[24] S. M. Rytov, Y. A. Kravtsov and V. I. Tatarskii, *Principles of Statistical Radiophysics* (Springer-Verlag, Berlin, 1989).

[25] D. Maystre, M. Hutley Opt.Commun, (1976).

[26] G. N. Zhizhin, E. A. Vinogradov, M. A. Moskalova and V. A. Yakovlev Appl. Spec. Rev. **18**, 171 (1982).

[27] P. J. Hesketh, J. N. Zemel and B. Gebhart, Nature (London) **324**, 549 (1986).

[28] P. J. Hesketh, J. N. Zemel and B. Gebhart, Phys. Rev. B **37**, 10795 (1988).

[29] P. J. Hesketh, J. N. Zemel and B. Gebhart, Phys. Rev. B **37**, 10803 (1988).

[30] F. Marquier, K. Joulain, J. P. Mulet, R. Carminati, J. J. Greffet and Y. Chen, *Phys. Rev. B*, **69**, 11 (2004)

[31] A. Heinzel, V. Boerner, A. Gombert, B. Blsi, V. Wittwer and J. Luther, *J. of Mod. Opt.*, **47**, 2399-2419 (2000)

[32] M. Laroche, C. Arnold, F. Marquier, R. Carminati, J. J. Greffet, S. Collin, N. Bardou and J. L. Pelouard, *Opt. Lett.*, **30**, 2623-2625 (2005)

[33] M. Laroche, F. Marquier, R. Carminati and J.-J. Greffet., *Opt. Commun.*, **250**, 316-320 (2005).

[34] F. Marquier, K. Joulain, J. P. Mulet, R. Carminati and J. J. Greffet, *Opt. Commun.*, **237**, 379-388 (2004)

[35] F. Marquier, M. Laroche, R. Carminati and J.J. Greffet, *J. of Heat Trans.*, **129**, 11-16 (2007)

[36] O.G. Kollyukh, A.I. Liptuga, V. Morozhenko and V.I. Pipa, *Opt. Commun.*, **225**, 349–352 (2003)

[37] A.I. Liptuga, *Infrared Physics and Technology*, **44**, 85–89 (2003)

[38] L. Hu, A. Schmidt, A. Narayanaswamy and G. Chen, *ASME J. Heat Transf.*, **126**, 786-792 (2004)

[39] I. Celanovic, D. Perreault and J. Kassakian, *Phys. Rev. B*, **72**, 075127 (2005)

[40] P. Ben-Abdallah and B. Ni, *J. Appl. Phys.*, **97**, 104910 (2005)

[41] B. J. Lee and Z.M. Zhang, *J. Appl. Phys.*, **100**, 063529 (2006)

[42] A. Battula and S.C. Chen, *Phys. Rev. B*, **74**, 245407 (2006)

[43] B.J. Lee and Z.M. Zhang, *ASME J. Heat Transf.*, **129**, 17-26 (2007)

[44] K. Joulain and A. Loizeau, *J. Quant. Spectrosc. Rad. Transfer*, **104**, 208-216 (2007)

[45] S. Maruyama, T. Kashiwa, H. Yugami and M. Esashi, *Appl. Phys. Lett.*, **79**, 1393-1395 (2001)

[46] M. U. Pralle, N. Moelders, M. P. McNeal, I. Puscasu, A. C. Greenwald, J. T. Daly, E. A. Johnson, T. George, D. S. Cho, I. El-Kady and R. Biswas, *Appl. Phys. Lett.*, **81**, 4685-4687 (2002)

[47] D.L.C. Chan, M. Soljacic and J.D. Joannopoulos, *Opt. Express*, **14**, 8785-8796 (2006)

[48] S. Enoch, J.J. Simon, L. Escoubas, Z. Elalmy, F. Lemarquis, P. Torchio and G. Albrand, *Appl. Phys. Lett.*, **86**, 261101 (2005)

[49] D.L.C. Chan, M. Soljacic and J.D. Joannopoulos, *Phys. Rev. E*, **74**, 036615 (2006)

[50] J.C.W. Lee and C.T. Chan, *Appl. Phys. Lett.*, **90**, 051912 (2007)

[51] H. Sai *et al.*, J. Opt. Soc. Am. A **18**, 1471 (2001).

[52] S. Y. Lin *et al.*, Nature (London) **394**, 6690 (1998)

[53] M. Auslender and S. Hava, Infrared Physics & Technology **36**, 1077 (1995).

[54] M. Auslender D. Levy and S. Hava, Appl. Opt. **37**, 369 (1998).

[55] D. Van Labeke, Gerard, D., B. Guizal, F.I. Baida and L. Li, *Opt. Expr.*, **14**, 11945-11951 (2006)

[56] S. Bauer, *American Journal of Physics*, **60**, 257-261 (1992)

[57] A.D. Parsons and D.J. Pedder, *Journal of Vacuum Science and Technology*, **6**, 1686-1689 (1987)

[58] J.J. Monzon and L.L. Sanchez, *Applied Optics*, **33**, 5137-5141 (1994)

[59] S. Chaudhuri, D. Bhattacharyya, A.B. Maity and A.K. Pal, *Materials Science Forum*, **246**, 181-206 (1997)

[60] C.G. Granqvist, *Advanced Materials*, **15**, 1789-1803 (2003)

[61] A. Dunlop, D. Lesueur, Radiation Effects and Defects in Solids **126** 123-128 (1993).

[62] D. Lesueur, A. Dunlop, Radiation Effects and Defects in Solids **126** 163-172 (1993).

[63] K. Joulain, J.P. Mulet, F. Marquier, R. Carminati, J.J. Greffet, Surf. Sci.Rep. **57**, 59-112 (2005)

[64] C. Kittel, *Introduction to Solid State Physics*, (John Wiley and Sons, New York, 1996).

[65] N. W. Ashcroft and N. D. Mermin, *Solid State Physics* (Saunders, Philadelphia, 1976).

[66] J.M. Ziman, *Electrons and Phonons*, (Oxford University Press, Oxford, 1960).

[67] H. Raether, *Surface Plasmons on Smooth and Rough Surfaces and on Gratings*, Vol. 111 of *Springer Tracts in Modern Physics* (Springer, Berlin, Heidelberg, 1988).

[68] V.M. Agranovitch and D.M. Mills, *Surface Polaritons*, (North-Holland, Amsterdam, 1982).

[69] E.N. Economou and K.L. Ngai, Adv.Chem.Phys. **27** p 265 (1974)

[70] Ed. A.D. Boardman, *Electromagnetic Surface Modes*, (John Wiley, New York, 1982).

[71] P. Halevi, Ed. A.D. Boardman, *Electromagnetic Surface Modes*, (John Wiley, New York, 1982).

[72] E.T. Arakawa and M.W. Williams and R.H. Ritchie, Phys. Rev. Lett. **31** p 1127 (1973)

[73] K.L. Kliewer and R. Fuchs, Adv. Chem. Phys. **27** p 355 (1974)

[74] A. Otto, Z. Phys. **241** p 398 (1971)

[75] E. Kretschmann, Z. Phys. **216** p 398 (1971)

[76] E.A.Vinogradov and G.N.Zhizhin and V.I.Yudson, Ed.V.M.Agranovich and D.L.Mills *Surface Polaritons*, (North Holland, Amsterdam, 1982).

[77] W.G. Spitzer, D. Kleinman and D. Walsh, Phys. Rev. **113** p 127 (1959)

[78] J.W. Goodman, *Statistical Optics*, (John Wiley and Sons, New York, 1985).